Journal of ELECTRONIC MATERIALS, Vol. 44, No. 10, 2015
DOI: 10.1007/s11664-015-3902-6

Preparation and Characterization of Zinc-Containing Nickel Gallate Ferrite

A. HASHHASH,[1,3,4] N.G. IMAM,[2] S.M. ISMAIL,[1] and M. YEHIA[1]

1.—Reactor Physics Department, Nuclear Research Center, Atomic Energy Authority, Cairo, Egypt. 2.—Experimental Physics Department, Nuclear Research Center, Atomic Energy Authority, Cairo, Egypt. 3.—e-mail: ee175sh@yahoo.com. 4.—e-mail: adelhashhash@gmail.com

Polycrystalline $Ni_{1-x}Zn_xFeGaO_4$ samples containing different amounts of zinc (x = 0.0, 0.1, 0.2, 0.3, 0.4, 0.5) were synthesized by solid-state reaction. Study of the crystal structure by x-ray diffraction (XRD) revealed peaks typical of a single-phase polycrystalline face-centered cubic structure (FCC). Elemental composition was determined by x-ray fluorescence (XRF) analysis. Fourier-transform infrared (FTIR) spectra contained two absorption bands related to the tetrahedral A and octahedral B sites of the spinel ferrite. Magnetization loops obtained by vibrating sample magnetometry (VSM) indicated that the saturation magnetization, M_s, decreased gradually with increasing in Zn content (x), and that coercivity H_c was related to the microstructure of the Zn-doped samples. Mössbauer effect (ME) spectra of the samples were broad and magnetically split for x = 0.0 and 0.1 and quadruple doublets for the other Zn^{2+} concentrations. The dielectric constant (ε') and dielectric loss tangent ($\tan\delta$) were also measured over wide ranges of frequency and temperature by use of the two probe method. The results were explained on the basis of cation–anion–cation and cation–cation interactions through the metal sites in the Ni–Zn–Ga ferrites.

Key words: Ni–Zn–Ga ferrite, XRD, FTIR, VSM, Mössbauer effect spectra, dielectric measurements

INTRODUCTION

Ferrites are magneto-dielectric ceramic materials with potential applications which include permanent magnets, memory-storage devices, and microwave devices. Ferrite materials are also used for manufacture of telecommunications equipment.[1] In the last few years there has been increasing interest in mixed ferrites, because of their interesting physical, chemical, and structural properties, and remarkably promising applications.[2] The spinel ferrites are an important group of magnetic materials, because of their useful magnetic properties, especially in the radiofrequency region, physical flexibility, high electrical resistivity, mechanical hardness, and chemical stability. Because of their excellent properties, much attention has also been devoted to mixed spinel ferrites, which are mainly used in electrical devices and as catalysts.[3] The structural, magnetic, and dielectric properties of a soft ferrite can be modified by adjustment of the type and amount of substituting elements it contains.[4] The Ni–Zn–Ga ferrite structure is classified as a soft ferrite and regarded as an important mixed magnetic material.[5] Substitution of spinel ferrites with nonmagnetic ions, for example zinc, has attracted much attention because it results in technologically important materials with high magnetic permeability and low core losses. The effects of such isomorphous substitution is particularly apparent from Mössbauer spectra, in which magnetic interactions are substantially reduced, which in turn reduces magnetic ordering and hyperfine fields.[6] In this work we studied the effect of introducing different concentrations of Zn^{2+} relative to the Ni^{2+} concentration into the ferrite

(Received January 9, 2015; accepted June 12, 2015; published online July 14, 2015)

$Ni_{1-x}Zn_xFeGaO_4$, where x ranges from 0.0 to 0.5 wt.%. The purpose was to obtain information about the structure, and magnetic and dielectric properties of these ferrites by use of x-ray diffraction (XRD), x-ray fluorescence (XRF), and Fourier-transform infrared (FTIR) spectroscopy, vibrating sample magnetometry (VSM), Mössbauer effect (ME) spectroscopy, and by measurement of the dielectric constant (ε') and dielectric loss tangent (tan δ). As we have reported elsewhere,[7] results from photoluminescence (PL) and structural characterization of Ni–Zn–Ga ferrite irradiated with γ-rays suggests potential use as a detector for γ-rays.

EXPERIMENTAL

Previously,[7] we successfully synthesized mixed spinel ferrites $Ni_{1-x}Zn_xFeGaO_4$ ($0.0 \le x \le 0.5$; step 0.1) from Fe_2O_3, ZnO, NiO, and Ga_2O_3 (purity 99.99%) by use of a double-sintering technique. In this work these samples were characterized by use of a Bruker D8 x-ray diffractometer with CuK_α radiation (λ = 1.5418). Elemental analysis was performed by energy-dispersive x-ray fluorescence spectrometry (Jeol JSX-3202EV). Fourier-transform Infrared (FTIR) spectra were recorded at room temperature in the frequency range 1000–200 cm^{-1} by use of a Jasco FTIR 310 spectrophotometer and the KBr disc technique. Magnetization measurements were performed by use of a vibrating sample magnetometer (VSM; 9600-1 LDJ, USA) with a maximum applied field of nearly 6 kOe at room temperature. An Austin Science Mössbauer spectrometer with a constant-acceleration laser-interferometer-controlled drive and data acquisition system was used in the standard transmission setup with a personal computer analyzer (PCA II-card-1024 channels).[3] The radioactive source was ^{57}Co imbedded in an Rh matrix with an initial activity of 50 mCi. A complex impedance technique with a two-probe method and model SR510 lock-in amplifier was used for determination of dielectric properties (ε' and tan δ) in the frequency and temperature ranges 10^2–10^5Hz and 293–510 K, respectively. Samples were pressed into pellets of diameter ~1 cm and thickness ~4 mm.[8] For measurement of electrical properties the two surfaces of each pellet were coated with silver paste and checked for good electrical contact.

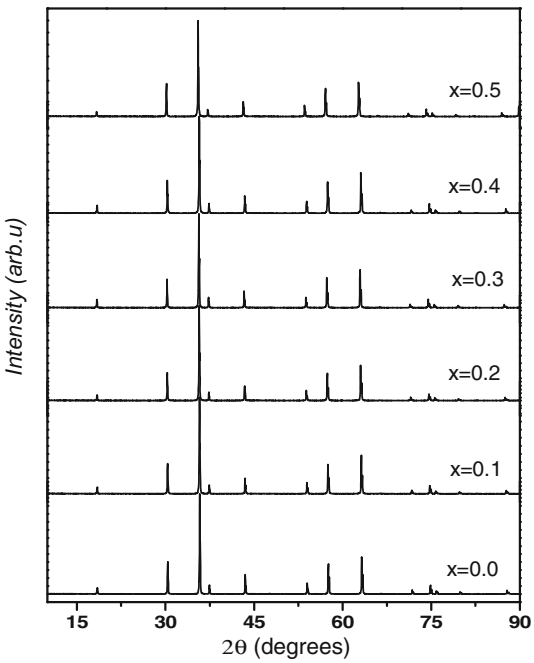

Fig. 1. Powder XRD patterns of $Ni_{1-x}Zn_xGaFeO_4$ ferrite samples with ($0.0 \le x \le 0.5$).

RESULTS AND DISCUSSION

XRD Analysis

Figure 1 shows XRD spectra of the samples; these confirm that pure $NiGaFeO_4$ and Zn-doped $Ni_{1-x}Zn_xGaFeO_4$ occur as single spinel phases. All the peaks in the XRD spectra were indexed by use of Bragg's law. The spectra contain no diffraction lines attributable to the presence of impurities or metal oxides. Values of the lattice constant a_{exp} and x-ray density $\rho_{x\text{-ray}}$ calculated from XRD data are summarized in Table I. The results show that a_{exp} for $Ni_{1-x}Zn_xGaFeO_4$ gradually increases with increasing x; this can be interpreted on the basis of cation distributions between the two crystallographic A and B sites, as is apparent from Mössbauer measurements (discussed below). In pure $NiGaFeO_4$ (x = 0.0) Ga^{3+} ions are equally distributed between A

Table I. Lattice constant, x-ray density $\rho_{x\text{-ray}}$, and FTIR absorption frequency bands for $Ni_{1-x}Zn_xGaFeO_4$ ferrites

Property	x = 0.0	x = 0.1	x = 0.2	x = 0.3	x =0.4	x = 0.5
Lattice constant, a_{exp} (Å)	8.315	8.322	8.330	8.347	8.335	8.341
$\rho_{x\text{-ray}}$ (g/cm^3)	5.737	5.738	5.737	5.717	5.757	5.760
High-frequency bands, v_1 (cm^{-1})	618	616	611	611	610	606
Low-frequency bands, v_2 (cm^{-1})	419	421	422	418	423	424

and B sites. Substitution of A sites with Zn^{2+}, a normal spinel ion with ionic radius $r_{tet.}$= 0.6 Å,[9] causes migration of Ga^{3+} ($r_{tet.}$= 0.47 Å) to B sites; as a result A sites expand. Replacement of Ni^{2+} ions in B sites ($r_{oct.}$= 0.69 Å) by migrating Ga^{3+} ions ($r_{oct.}$ = 0.62 Å) causes compression of the octahedral B sites in the Ni–Zn–Ga ferrite. The final result of these substitutions is a slight increase of a_{exp} (Table I). An anomalous increase in a_{exp} at the point x = 0.3 may be because of replacement of Ni^{2+} ions ($r_{oct.}$ = 0.69 Å) by Zn^{2+} ions ($r_{oct.}$ = 0.74 Å) at B sites. The x-ray density can be calculated as $\rho_{x\text{-}ray} = 8M/N_A a^3_{exp}$, where M is molecular weight, N_A is Avogadro's number, and a_{exp} is the lattice constant. The values of x-ray density $\rho_{x\text{-}ray}$ change as follows:

1. $\rho_{x\text{-}ray}$ decreases as a result of the slight increase in a_{exp}; and
2. $\rho_{x\text{-}ray}$ increases as the concentration of Zn^{2+} ions increases, because Zn^{2+} ions are heavier than Ni^{2+} ions (Table I).

X-ray Fluorescence (XRF) Spectrometry

The stoichiometry of the $Ni_{1-x}Zn_xFeGaO_4$ samples was investigated by XRF analysis. The XRF spectra Fig. 2 indicated the presence of Ga, Ni, Zn, and Fe as major elements in the material, with no impurities. These results reveal that the precursors have completely undergone chemical reaction to

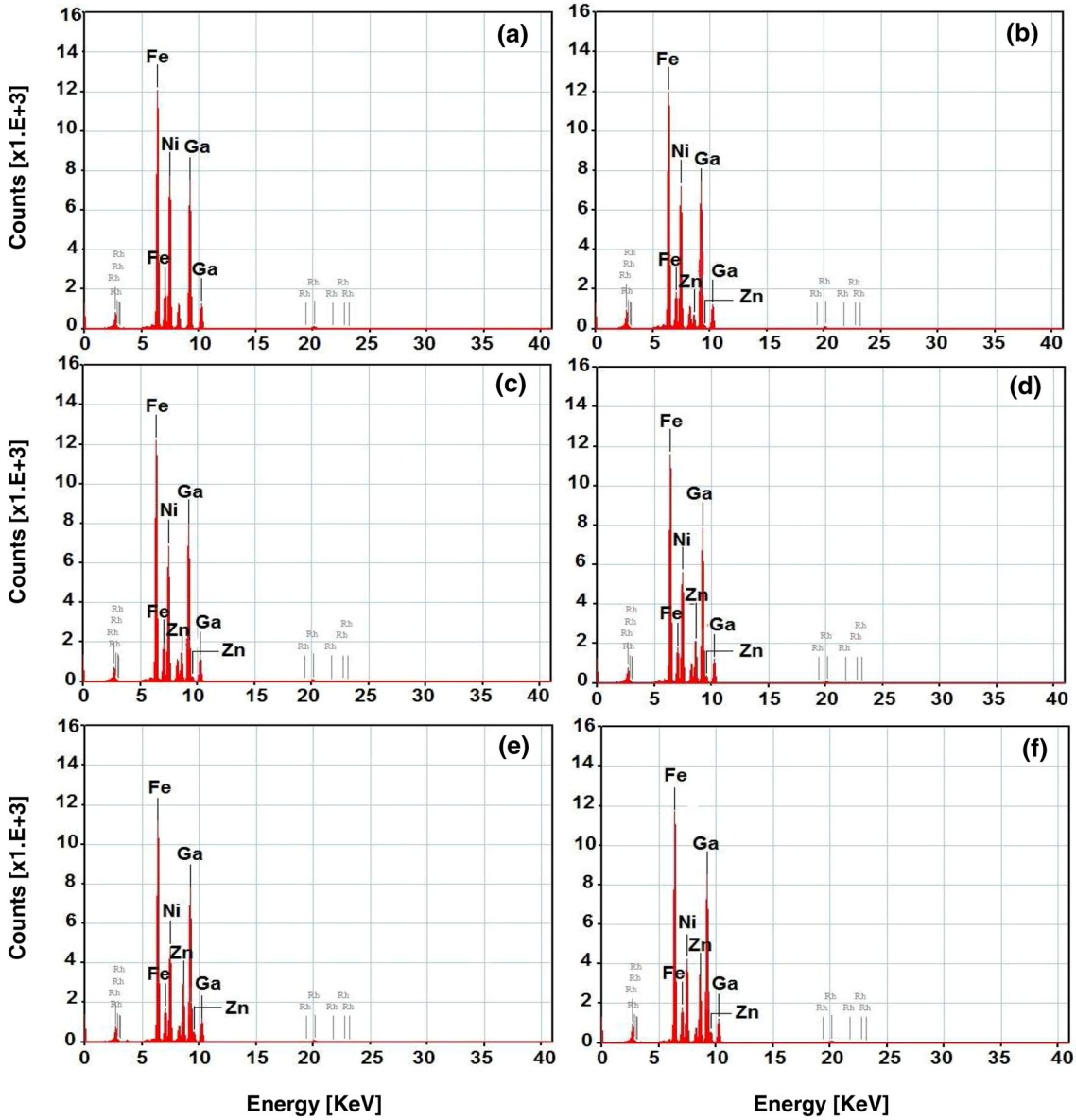

Fig. 2. X-ray fluorescence spectra XRF of $Ni_{1-x}Zn_xGaFeO_4$ ferrite samples (a) x = 0.0, (b) x = 0.1, (c) x = 0.2, (d) x = 0.3, (e) x = 0.4, (f) x = 0.5.

form the expected ferrites. Table II shows the ratios from XRF elemental analysis of Ga, Fe, Ni, and Zn ions, which are very close to the stoichiometric values. These results reflect the level of homogeneity and are evidence that the composition of the samples used in this work is uniform; furthermore the ratios obtained precluded the possibility of uneven distribution of Zn throughout the samples.

FTIR Study

FTIR spectra of the Ni–Zn–Ga ferrites in the range 1000–200 cm^{-1} (Fig. 3) contain two absorption bands. The broad peaks correspond to vibration of the tetrahedral and octahedral complexes because of formation of the spinel ferrite structure.[10] The higher and lower absorption bands (ν_1 and ν_2) in the ranges 606–618 cm^{-1} and 418–424 cm^{-1} (Table I) are attributed to the stretching vibration of the unit cell at the A and B sites, respectively. These two bands are caused by vibration of metal–oxygen complexes at the two crystallographic sites.[11,12] Substitution of Ga^{3+} by Zn^{2+} in an A site causes a decrease in the bond length and, consequently, a decrease in the vibration frequency at the A site.[13,14] Moreover, migration to B sites of Ga^{3+} ions with ionic radii smaller than those of Ni^{2+} increases the bond length and, consequently, increases the frequency of vibration (Table I).

Mössbauer Measurements

Figure 4 shows room-temperature Mössbauer effect (ME) spectra for the $Ni_{1-x}Zn_xGaFeO_4$ samples ($0.0 \le x \le 0.5$). Two split Zeeman sextets are obtained, because of the presence of Fe^{3+} at A and B sites in the $NiGaFeO_4$. However, two magnetically broad Zeeman sextets with a quadruple duplets are observed for the sample with (x = 0.1). Otherwise and for further increasing amounts of Zn^{2+} ions ($x \ge 0.2$), quadruple duplets are clearly observed (Fig. 4). On the basis of site-preference energy data,[5] the two elements Zn^{2+} and Ni^{2+} occupy the A and B sites, respectively. The cation distribution estimated from the ME spectra for the two samples with x = 0.0 and 0.1 are $(Ga_{0.5}Fe_{0.5})[NiGa_{0.5}Fe_{0.5}]O_4$ and $(Zn_{0.1}Ga_{0.4}Fe_{0.5})[Ni_{0.9}Ga_{0.6}Fe_{0.5}]O_4$ respectively, where ( ) refers to the tetrahedral A site and [ ] refers to the octahedral B site. Fe^{3+} was equally

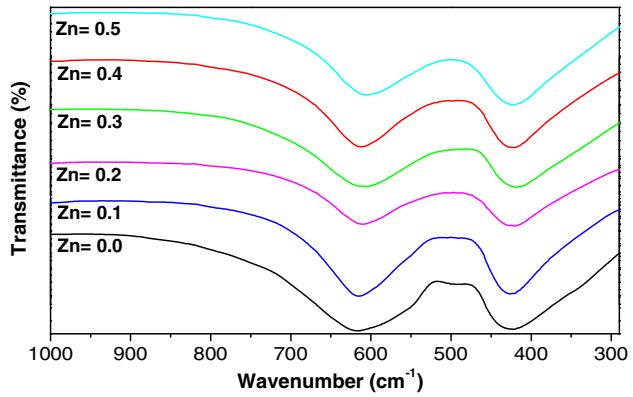

Fig. 3. FTIR spectra of $Ni_{1-x}Zn_xGaFeO_4$ ferrite.

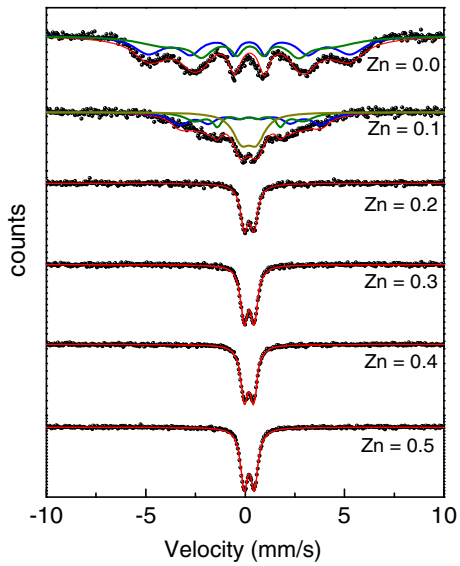

Fig. 4. Mössbauer spectra of Ni–Zn–Ga ferrite at room temperature.

Table II. Elemental composition of $Ni_{1-x}Zn_xGaFeO_4$ determined by XRF

x	Composition of elements	Fe^{3+}	Ga^{3+}	Ni^{2+}	Zn^{2+}
0.0	Value for stoichiometric compound	1	1	1	0
	XRF analysis	1.07	1.11	1.02	0
0.1	Value for stoichiometric compound	1	1	0.9	0.1
	XRF analysis	1.07	1.11	0.93	0.11
0.2	Value for stoichiometric compound	1	1	0.8	0.2
	XRF analysis	1.06	1.12	0.82	0.21
0.3	Value for stoichiometric compound	1	1	0.7	0.3
	XRF analysis	1.06	1.11	0.71	0.31
0.4	Value for stoichiometric compound	1	1	0.6	0.4
	XRF analysis	1.04	1.12	0.60	0.43
0.5	Value for stoichiometric compound	1	1	0.5	0.5
	XRF analysis	1.06	1.13	0.52	0.48

distributed between the two crystallographic A and B sites. In addition the distribution of cations for the remaining samples of the series, $x \geq 0.2$, can be estimated on the basis of the VSM results (discussed later) as $(Zn_xGa_{0.5-x}Fe_{0.5})[Ni_{1-x}Ga_{0.5+x}Fe_{0.5}]O_4$. This indicates that substitution of Zn^{2+} in the A site causes migration of Ga^{3+} from the A site to the B site. FTIR results also support this estimated distribution of the cations. For the two samples with Zn concentrations $x = 0.0$ and 0.1 hyperfine field values for Fe^{3+} ions located in the A site (Hf_A) are smaller than for these ions in the B site (Hf_B) (Fig. 5). The paramagnetic doublet, i.e. no distinct separation of the hyperfine fields, observed for samples with $x \geq 0.2$ can be associated with blocking of spin clusters in the superparamagnetic state.[3] However the values of the isomer shift (δ) for all the samples in the range 0.14–0.24 mm/s are consistent with iron ions in the trivalent state.[15] In agreement with the correlation between the hyperfine field and the isomer shift, the Zeeman patterns with smaller hyperfine field (Hf_A) have smaller isomer shifts (δ_A).[5] In our Ni–Zn–Ga-ferrites the presence of two nonmagnetic elements, Ga^{3+} and Zn^{2+}, in the unit cell increases the height of the energy barriers and increases the relaxation effect in the ME spectra.[15,16] The values of quadruple splitting (Q_S) for the two samples with $x = 0.0$ and 0.1, are close to zero (Fig. 5), which is indicative of cubic symmetry of the spinel phase. Otherwise the presence of quadruple splitting (Q_S) for samples with higher Zn concentrations ($x \geq 0.2$) is mainly because of chemical disorder, which produces an electric field gradient (EFG) of different magnitude, direction, sign and symmetry. In this work the presence of Q_S arises from the asymmetric charge distribution around iron in both A and B sites.[16]

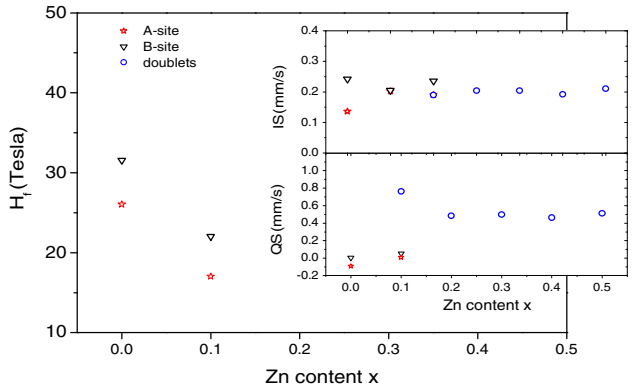

Fig. 5. ME results for Ni–Zn–Ga ferrite at room temperature.

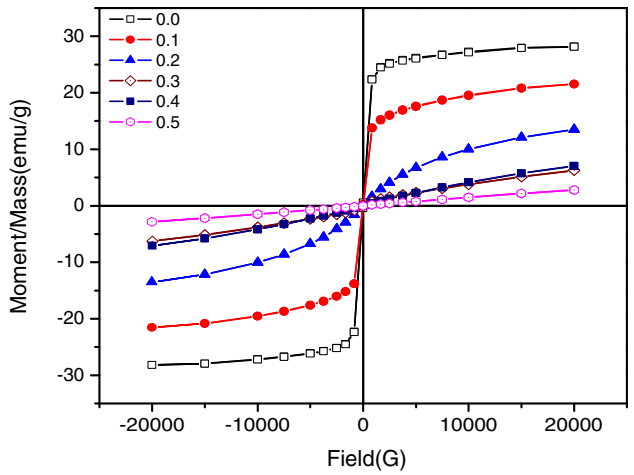

Fig. 6. Room-temperature hysteresis curves of $Ni_{1-x}Zn_xGaFeO_4$ ferrite.

VSM Measurements

Figure 6 shows the magnetization curves (M–H) obtained for the mixed ferrite $Ni_{1-x}Zn_xGaFeO_4$ at room temperature. Hysteresis is absent and ferromagnetic behavior of the samples is not observed got high concentrations of Zn^{2+} ($0.3 \leq x \leq 0.5$). Saturation magnetization, M_s, is not reached for all the samples even at a maximum applied field of 20 kG. Consequently, M_s can be calculated by use of the equation[17] $M = M_s(1 - a/H)$, where (M, H and a) are the magnetization, applied magnetic field, and a fitting term, respectively. The saturation magnetization

Table III. Magnetic data and activation energy of Ni–Zn–Ga ferrite

x	M_s (emu/g)	H_c (G)	μ_o Bohr magneton	μ_c Bohr magneton	Activation energy E_a (eV)
0.0	28.19	18.04	1.25	2.0	0.447
0.1	21.55	8.01	0.96	1.8	0.482
0.2	13.53	5.94	0.61	1.6	0.516
0.3	7.10	17.24	0.32	1.4	0.523
0.4	6.24	28.54	0.28	1.2	0.536
0.5	2.88	46.48	0.13	1.0	0.553

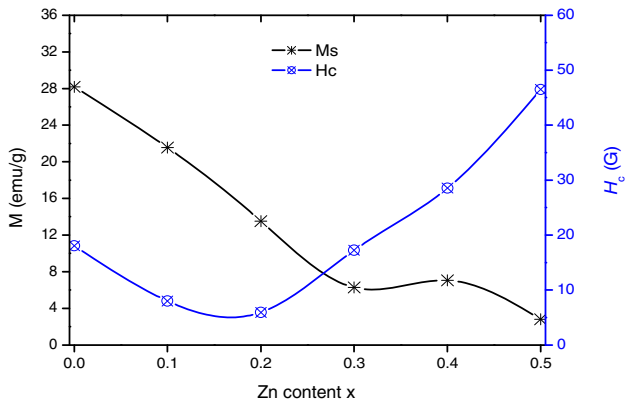

Fig. 7. Dependence of magnetization (M_s) and coercivity (H_c) on Zn concentration.

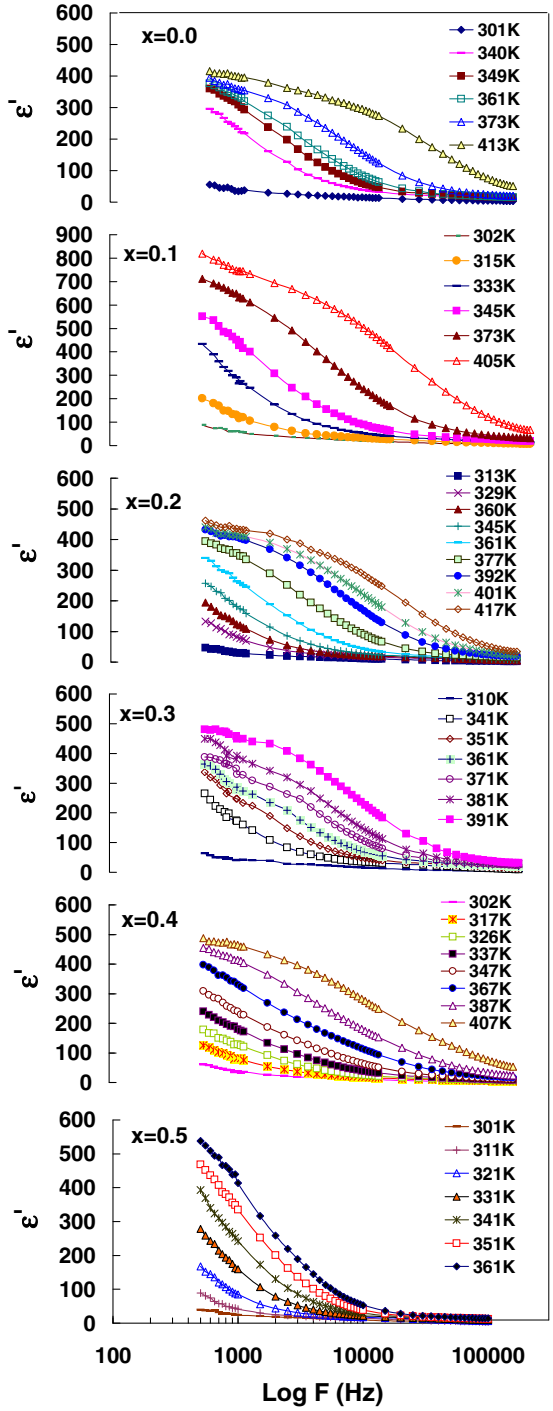

Fig. 8. ε' as a function of frequency (log f) at different temperatures for $Ni_{1-x}Zn_xGaFeO_4$.

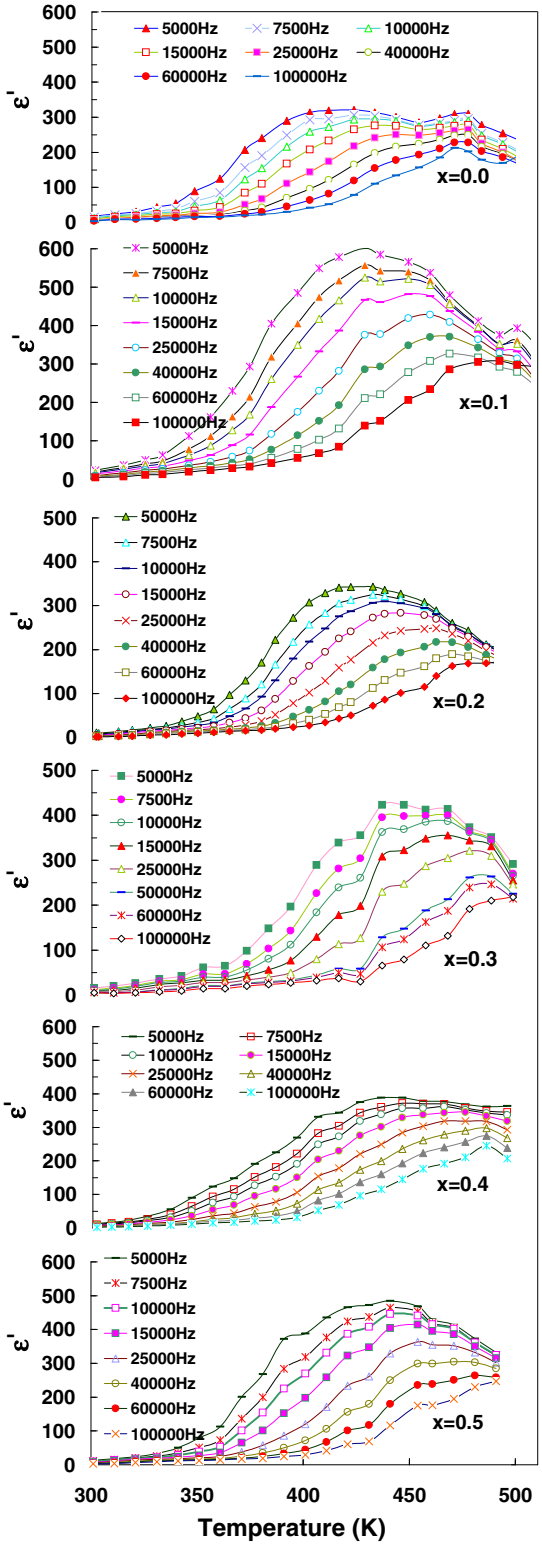

Fig. 9. Temperature dependence of ε' at different frequencies for $Ni_{1-x}Zn_xGaFeO_4$.

can be obtained from the straight line relationship between M and $1/H$ in the high-field region. The intercepts of the lines with the M-axis give the M_s values summarized in Table III with other magnetic data. The values of the saturation magnetization M_s and coercivity H_c are plotted against Zn-content (x) Fig. 7. Nandapure et al. reported[11] that M_s for Zn^{2+}-substituted $NiFe_2O_4$ increased with increasing concentration of Zn^{2+}. The reason is migration of Fe^{3+} ion to B sites as a result of the substitution of Zn^{2+} in A sites. This gives rise to antiparallel spin coupling and spin canting, resulting in weakening of

the A–B exchange interaction. In our work M_s values gradually decreased on substitution with Zn^{2+} (Fig. 7 and Table III). This can be attributed to migration of the non-magnetic Ga^{3+} ion with the $3d^{10}$ configuration from A sites to B sites, which causes blocking of spin clusters in the superparamagnetic state and increasing the height of energy barriers. Consequently both A–B and B–B superexchange interactions are reduced.[12] It is apparent from Fig. 7 that coercivity H_c decreases with increasing Zn^{2+} concentration and reaches a minimum value at $x = 0.2$. A gradual increase in H_c is observed on further increasing the concentration of Zn^{2+} ($x \geq 0.3$). In general the magnetic coercivity H_c changes, because of the effect of cationic stoichiometry and the distribution of the metals in the crystallographic sites. This result can be interpreted on the basis of magnetocrystalline anisotropy, which mainly depends on the distributions of the magnetic moments of the ions on the surfaces of the particles. Superparamagnetic behavior of our samples was also observed, because of the presence of nonmagnetic Ga^{3+} and Zn^{2+} ions.[18] Moreover, the very low values of H_c (Table III) are because of the presence of soft magnetic materials.[19–21] The observed magnetic moment, μ_o, can be calculated by use of the formula[13] $\mu_o = MWM_s/5585$, where MW is molecular weight and M_s is the saturation magnetization in emu/g (Table III). According to Neel's two sub-lattice model of ferrimagnetism[22,23] the calculated magnetic moment μ_c can be expressed as $\mu_c = M_B - M_A$, where M_A and M_B are the A and B sub-lattice magnetic moments, respectively. On the basis of the estimated cation distribution and the values of the magnetic moments of the ions, Fe^{3+} ($5\mu_B$), Ni^{2+} ($2\mu_B$), Ga^{3+} ($0\mu_B$), and Zn^{2+} ($0\mu_B$), the values of μ_c can be calculated; these are listed in Table III. Replacement of Ni^{2+} ions by Zn^{2+} ions causes migration of Ga^{3+} ions from A sites to B sites which, in turn, reduces B-sub-lattice magnetization. These substitutions reduce the values of both calculated, μ_c, and observed, μ_o, magnetic moments as the concentration of Zn^{2+} increases (Table III).

Dielectric Properties

Dielectric constant (ε') as a function of the logarithm of frequency (log f) at different temperatures

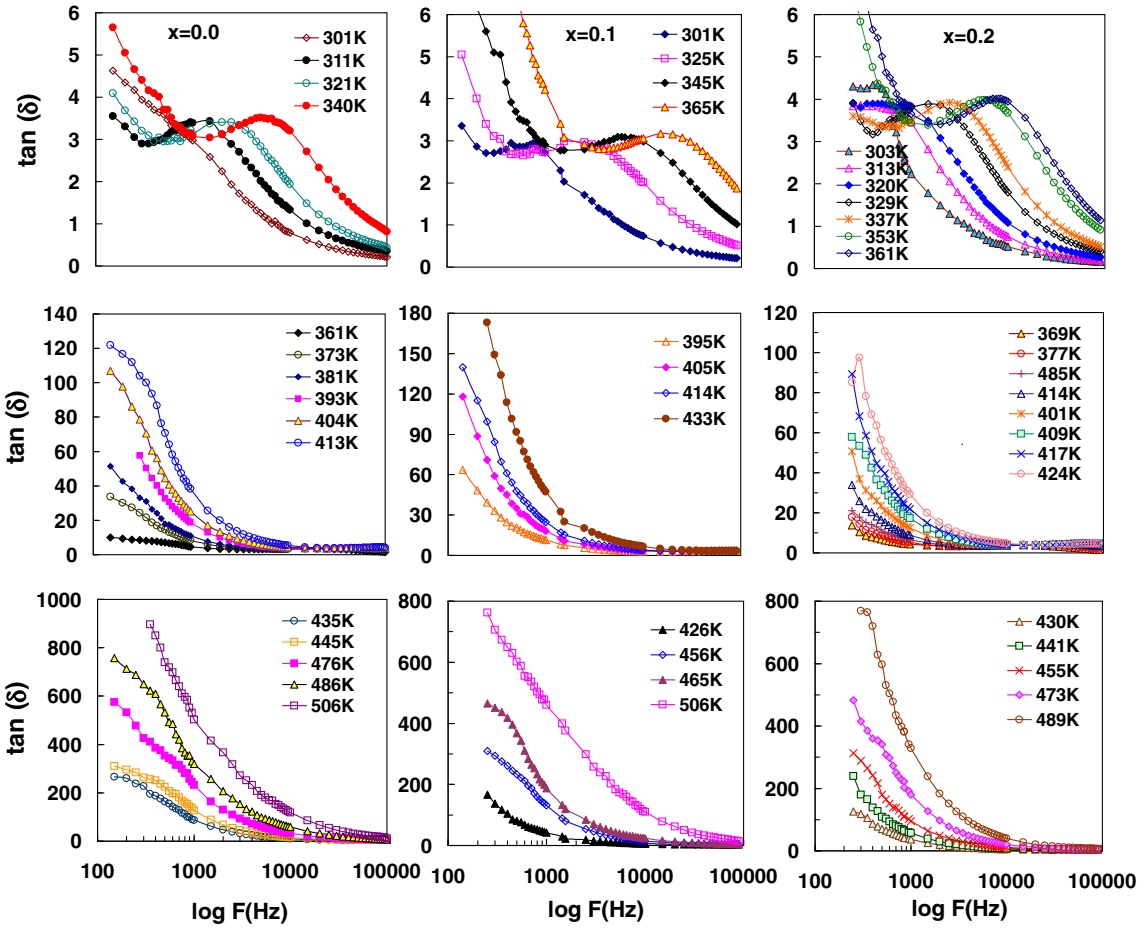

Fig. 10. Tan δ as a function of frequency (log f) for Ni–Zn–Ga ferrites at different temperatures.

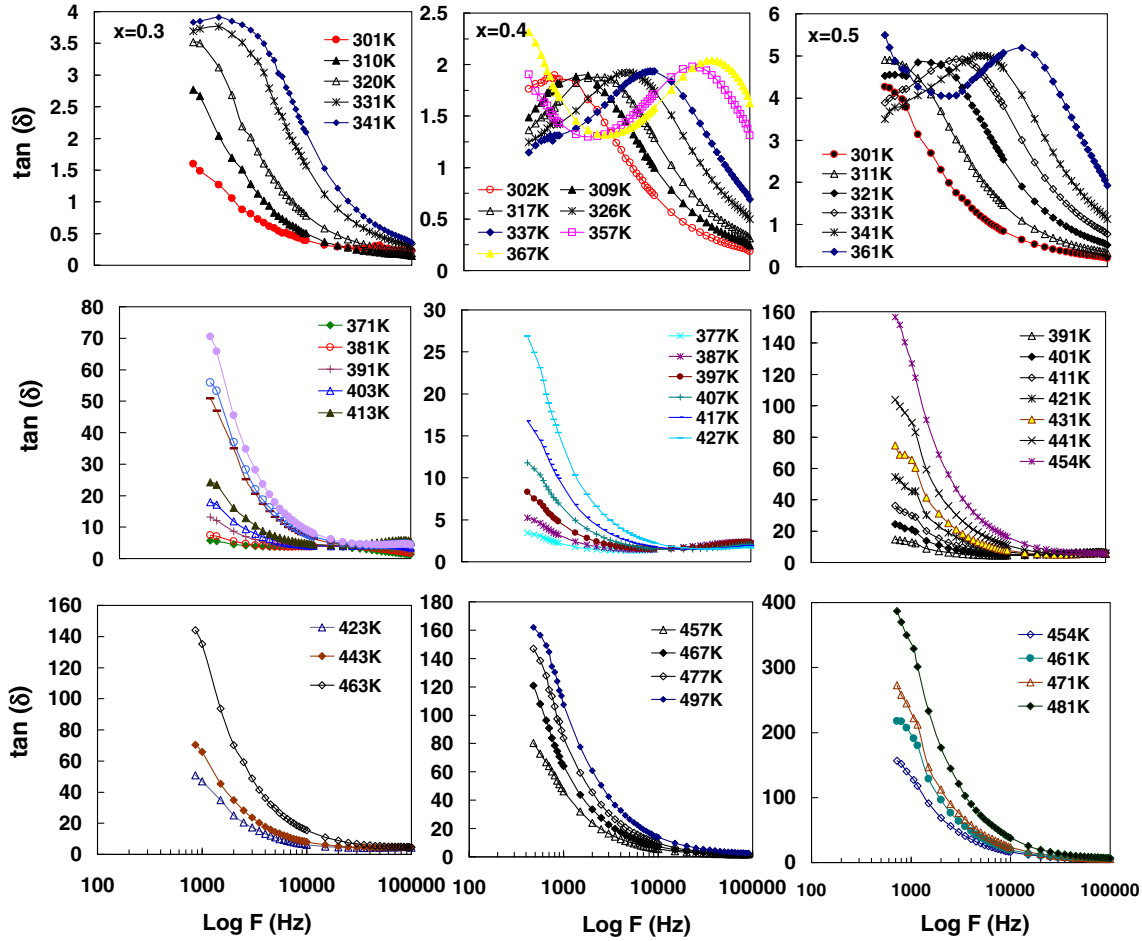

Fig. 10. continued.

for the ferrite $Ni_{1-x}Zn_xGaFeO_4$ is shown in Fig. 8. The behavior of the samples is similar to that of most ferrites.[6,8,15] Dispersion behavior is observed for ε' at low frequencies, and becomes frequency-independent at high frequency. It is also observed from Fig. 8 that on increasing the concentration of Zn^{2+}, dispersion of ε' values is shifted to lower frequencies. The reduction of ε' on increasing the frequency of the applied field can be interpreted on the basis of the Koop and Maxwell–Wagner phenomena.[13,24] Frequency-independent behavior is observed because of the inability of the electric dipoles to harmonize with the increasing frequency of the applied field. Four types of polarization, ionic (P_i), electronic (P_e), dipolar (P_d), and space charge (P_s) polarization, are present at low frequency, which is the reason for the large values of ε'. The total polarization (P_t) at low frequency is the sum of these four types, i.e., $P_t = P_i + P_e + P_d + P_s$. Beyond a specific frequency of the external applied field hopping of electrons is disabled, and polarization decreases to a constant value with increasing frequency.[25] Accordingly, the decrease in the dielectric constant on increasing the frequency is because of the low polarization. Primary losses in ferrites are because of hysteresis and eddy current at the functioning frequency, which is lower than the relaxation frequency of wall dislocation.[13] In our ferrites $Ni_{1-x}Zn_xGaFeO_4$, the rate of collapse of ε' is increased by substitution of Zn^{2+}, because of increasing disorder in the system. As previously mentioned, addition of Zn^{2+} to A sites causes migration of Ga^{3+} ($3d^{10}$) from A sites to B sites which, in turn, isolates the Fe^{3+} ions in B sites and reduces n-type conduction (hopping of electrons between Fe^{3+} and Fe^{2+}). The gradual decrease of Ni^{2+} in B sites also reduces p-type conduction (hopping of holes between Ni^{3+} and Ni^{2+}). These two types of hopping in B sites explain the polarization in our ferrites.[24] The relationship between ε' and temperature at different frequencies is shown in Fig. 9. It is apparent that in this temperature range ($330 \le T \le 480$ K), the dielectric constant ε' has sensitive temperature and frequency dependence. Maximum peaks are also observed, and are shifted to higher temperature with increasing concentration of Zn^{2+}. Figure 9 shows ε' is frequency-independent at temperatures below 330 K and above 480 K. The dependence of ε' on temperature can be explained on the basis of the existence of dipolar and interfacial

polarization, which are sensitive to changes in temperature.[25] On increasing the temperature the charges are accumulated at the grain boundary, which increases the polarization and consequently encourages accumulation of more charges. Figure 10 shows plots of dielectric loss tangent (tan δ) as a function of the logarithm of frequency (log f) for the $Ni_{1-x}Zn_xGaFeO_4$ spinels in the temperature range $330 \le T \le 480$ K. Each column represents one composition (x) and is divided into three plots for three different temperature ranges. In the lower range of temperature (310–365 K), dielectric loss tangent (tan δ) is frequency and temperature-dependent with observed loss peaks. On increasing the temperature, in the range 310–365 K the loss peaks are shifted to higher frequency. In the high-temperature range (366–510 K) the loss peaks are absent. In addition dispersion of the values of tan δ are observed at low frequencies; tan δ then becomes frequency-independent above 20 kHz.[26–28] These results can be interpreted on the basis of the strong correlation between tan δ and the type of conduction mechanism in the spinel ferrites.[8] The conduction mechanism is mainly depends on the hopping process in the octahedral B site, and a maximum loss peak is observed when the frequency of the external field is equal to the frequency of the hopping process. Ata-Allah[29,30] explained that both cation–cation and cation–anion–cation interactions occur in the spinel ferrite because of the presence of transition metal ions in the B sites. For high-spin-transition metal ions (number of electrons in the d orbital >5) the cation–anion–cation interaction is prevalent at the B sites. The cation–anion–cation interaction is between the wave function of the 3d orbital of the transition metal element and the wave function of the 2p orbital of oxygen, and it is stimulated by applying an alternating electric field. In our ferrites, substitution of Zn^{2+} ($3d^{10}$) in A sites causes migration of Ga^{3+} ($3d^{10}$) from A sites to B sites, which consequently reduces the cation–anion–cation interaction (Fe^{3+}–O^{2-}–Fe^{3+}) in the octahedral B site. These substitutions in our Ni–Zn–Ga ferrites lead to shift of the loss peaks to higher frequencies on increasing the concentration of Zn^{2+} Fig. 10.

The dielectric loss tangent can be given as a function of frequency and relaxation time as[8]:

$$\tan\delta = \frac{1}{\omega\tau} \tag{1}$$

and the relaxation time is given as a function of temperature as[31]:

$$\tau = \tau_0 \exp\left(-\frac{E_a}{K_B T}\right) \tag{2}$$

where ω ($= 2\pi f$) is the angular frequency, τ is the relaxation time ($\tau_0 = 1/1\upsilon_\infty$), υ_∞ is the maximum frequency, E_a is the activation energy of the relaxation process, k_B is Boltzmann's constant, and T is the absolute temperature. In the relationship between tan δ and log f a maximum occurs when the frequency of the applied alternating field harmonizes with the frequency of hopping of the charge carriers. The values of the relaxation time τ can be calculated from Fig. 10 considering that at the maximum loss $\omega\tau = 1$.[8,31] The activation energy E_a can be calculated from a plot of ln τ against the reciprocal of the absolute temperature Fig. 11; the values are listed in Table III. The straight line plot shows the existence of one relaxation process related to AC conductivity. It is clear that E_a increases on increasing the concentration of Zn^{2+} (Table III). This can be interpreted as the result of transfer of Ga^{3+} from A sites to B sites on addition of Zn^{2+}.

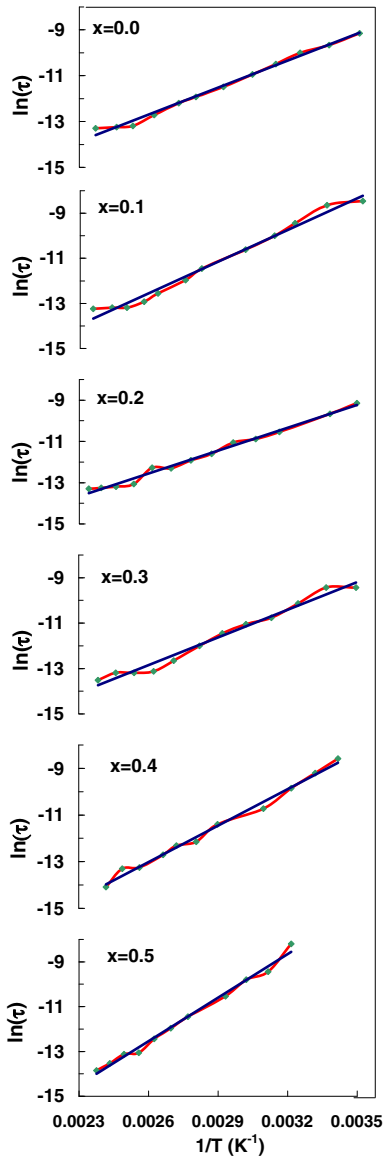

Fig. 11. Relaxation time lnτ as a function of $1/T$ for $Ni_{1-x}Zn_xGaFeO_4$ ferrites.

CONCLUSION

Ni–Zn–Ga ferrites were successfully prepared by solid-state reaction. XRD confirmed formation of a single FCC structure. Lattice constants increased slightly with increasing Zn^{2+} concentration. FTIR results for the two crystallographic sites were in agreement with the estimated cation distribution. ME spectra for the first two samples in the series (x = 0.0, 0.1) contained two split Zeeman sextets, because of the presence of Fe^{3+} at the A and B sites; quadruple duplets were observed for the other samples ($x \geq 0.2$). Saturation magnetization was not reached, even with a maximum applied field of 20 kG. ε' and tan δ were strongly correlated with Zn^{2+} concentration. Addition of Zn^{2+} caused migration of Ga^{3+} to B sites which, in turn, isolated the Fe^{3+} ions and reduced n-type and p-type conduction.

REFERENCES

1. K. Mohit, S.K. Rout, S. Parida, G.P. Singh, S.K. Sharma, S.K. Pradhan III, and W. Kim, *Phys. B* 407, 935 (2012).
2. M. Tana, Y. Koseoglua, F. Alana, and E. Senturk, *J. Alloys Compd*. 509, 9399 (2011).
3. S.S. Ata-Allah, M.K. Fayek, and M. Yehia, *J. Magn. Magn. Mater.* 279, 411 (2004).
4. S.S. Ata-Allah, *J. Solid State Chem.* 177, 4443 (2004).
5. M.A. Ahmed, N. Okasha, and N.G. Imam, *The 7th African Rev. of Phys*. (ICTP, Italy, 2012).
6. S.S. Ata-Allah and M. Yehia, *Phys. B* 404, 2382 (2009).
7. N.G. Imam and A. Hashhash, *Nucl. Instrum. Methods. A* 767, 353 (2014).
8. S.S. Ata-Allah, M.K. Fayek, H.A. Sayed, and M. Yehia, *Mater. Chem. Phys.* 92, 278 (2005).
9. A. Hashhash, M. Yehia, S.M. Ismail, and S.S. Ata-Allah, *J. Supercond. Nov. Magn.* 27, 2305 (2014).
10. M.A. Gabal, R.S. Al-Luhaibi, and Y.M. AlAngari, *J. Magn. Magn. Mater.* 348, 107 (2013).
11. A.I. Nandapure, S.B. Kondawar, P.S. Sawadh, and B.I. Nandapure, *Phys. B* 407, 1104 (2012).
12. M.A. Gabal, S.A. Al-Thabaiti, E.H. El-Mossalamy, and M. Mokhtar, *Ceram. Int.* 36, 1339 (2010).
13. M. Hashim, Alimuddin, S.E. Shirsath, S. Kumar, R. Kumar, A.S. Roy, J. Shah, and R.K. Kotnala, *J. Alloys Compd*. 549, 348 (2013).
14. M.A. Gabal, R.M. El-Shishtawy, and Y.M. AlAngari, *J. Magn. Magn. Mater*. 324, 2258 (2012).
15. S.S. Ata-Allah, *J. Magn. Magn. Mater.* 284, 227 (2004).
16. S.S. Ata-Allah, M.K. Fayek, H.S. Refai, and M.F. Mostafa, *J. Solid State Chem.* 149, 434 (2000).
17. G. Dixit, J. PalSingh, R.C. Srivastava, and H.M. Agrawal, *J. Magn. Magn. Mater*. 324, 479 (2012).
18. O.M. Lemine, M. Bououdina, M. Sajieddine, A.M. Al-Saie, M. Shafi, A. Khatab, M. Alhilali, and M. Henini, *Phys. B* 406, 1989 (2011).
19. P.P. Hankare, R.P. Patil, A.V. Jadhav, K.M. Garadkar, and R. Sasikala, *Appl. Catal. B Environ.* 107, 333 (2011).
20. A.E. Berkowitz, R.H. Kodama, S.A. Makhlouf, F.T. Parker, F.E. Spada, E.J. Mcniff, and S. Foner, *J. Magn. Magn. Mater.* 196, 594 (1999).
21. V. Sepelak, L. Wilde, U. Steinike, and K.D. Becker, *Mater. Sci. Eng. A* 865, 375 (2004).
22. M.A. Gabal, A.M. Abdel-Daiem, Y.M. Al Angari, and I.M. Ismail, *Polyhedron* 57, 105 (2013).
23. M. Sertkol, Y. Kseoglu, A. Baykal, H. Kavas, A. Bozkurt, and M.S. Toprak, *J. Alloys Compd.* 486, 325 (2009).
24. M.A. Khan, M. ul Islam, M. AsifIqbal, M. Ahmad, M.F. Din, G. Murtaz, I. Ahmad, and M.F. Warsi, *Ceram. Int*. 40, 3571 (2014).
25. A.S. Fawzi, A.D. Sheikh, and V.L. Mathe, *J. Alloys Compd*. 502, 231 (2010).
26. D. Ravinder, G.R. Mohan, Prankishan, Nitendarkishan, and D.R. Sagar, *Mater. Lett*. 44, 256 (2000).
27. H. Ismael, M.K. El-Nimr, A.M. Abou El Ata, M.A. El Hiti, M.A. Ahmed, and A.A. Murakhowskii, *J. Magn. Magn. Mater.* 150, 403 (1995).
28. M.A. El Hiti, M.A. Ahmed, M.M. Mosaad, and S.M. Attia, *J. Magn. Magn. Mater.* 150, 399 (1995).
29. S.S. Ata-Allah and M.K. Fayek, *Phys. Stat. Sol. (a)* 175, 725 (1999).
30. S.S. Ata-Allah, *Mater. Chem. Phys.* 87, 378 (2004).
31. M. Hashim, Alimuddin, S. Kumar, S.E. Shirsath, E.M. Mohammed, H. Chung, and R. Kumar, *Phys. B* 407, 4097 (2012).